Available online at www.sciencedirect.com

SciVerse ScienceDirect

Ceramics International 39 (2013) 8245–8251

CERAMICS INTERNATIONAL

www.elsevier.com/locate/ceramint

Effects of extra Ba^{2+} and two-step sintering on the crystal structure, microstructure, and dielectric properties of (Ba, Ca)(Ti, Zr)O_3

Che-Yuan Chang*, Hsin-I Ho, Tsung-Yu Hsieh, Chi-Yuen Huang*, Yu-Chun Wu

Department of Resources Engineering, National Cheng Kung University, One University Road, Tainan 701, Taiwan

Received 25 February 2013; received in revised form 3 April 2013; accepted 3 April 2013
Available online 9 April 2013

Abstract

This study investigated how extra Ba^{2+} and two-step sintering affect the crystal structure, microstructure, and dielectric properties of (Ba, Ca)(Ti, Zr)O_3 (BCTZ). XRD results indicate that no secondary phase formed in any of the BCTZ samples after sintering. Raman spectra reveal that Ca^{2+} ions were pushed from the Ba-site to the Ti-site when extra Ba^{2+} was added after sintering. The Curie temperatures of all BCTZ samples decreased due to the smaller tetragonality caused by the addition of extra Ba^{2+}. SEM micrographs revealed that two-step sintering decreased the grain size from 5.0 μm to 0.5 μm compared with normal sintering. Furthermore, samples with fine-grain microstructures exhibited flat curves for the temperature coefficient of capacitance.

Keywords: $BaTiO_3$; Raman; Cell parameters; Two-step sintering; TCC curves

1. Introduction

As a ferroelectric perovskite ceramic, barium titanate ($BaTiO_3$) exhibits a high permittivity at room temperature, making it suitable for applications in multi-layer ceramic capacitors (MLCCs). However, the permittivity of pure $BaTiO_3$ ceramics changes dramatically with temperature, particularly near the phase transition temperatures (−90 °C, 0 °C, and 125 °C), especially the Curie temperature ($T_c \sim 125$ °C). Unstable changes in permittivity at the phase transition temperature cause damage in electric devices. Many studies have cited internal stress as the main factor affecting the temperature coefficient of the capacitance curve, caused by either a core–shell structure or a fine-grain microstructure. Previous studies have demonstrated that a stable temperature coefficient of capacitance (TCC) can be obtained by increasing T_c with the addition of rare earth oxides to reduce the dramatic changes in permittivity at T_c [1–5]. The increase in T_c is attributed to the changes in internal stress caused by the substitution of rare earth elements in the shell region of a $BaTiO_3$ surface, referred to as a "core–shell" structure. Otherwise, reducing the grain size to a "non-core shell" structure increases the internal stress and decreases the tetragonality, subsequently decreasing the spontaneous polarization. The TCC curve can be broadened by decreasing the spontaneous polarization. Additionally, $BaTiO_3$ can be modified by many dopants e.g., $CaCO_3$, ZrO_2, MgO, MnO, Bi_2O_3, and Nb_2O_5, to obtain a high dielectric constant and a broadened TCC curve [6–9].

The Curie temperature is also related to the tolerance factor (t_f), which is indicated by the degree of lattice distortion. A t_f close to 1 refers to a nearly cubic structure. Previous studies have found a general trend towards higher transition temperatures with a decreasing tolerance factor in ferroelectric perovskites [10]. Evidently, solid solutions of $BiScO_3$ (t_f=0.907), $BiInO_3$ (t_f=0.884), and $BiYbO_3$ (t_f=0.857) with $PbTiO_3$ (t_f=1.019) exhibit morphotropic phase boundaries (MPBs) with T_c values that are significantly higher than those of PZT (T_c=386 °C) and $PbTiO_3$ (T_c=490 °C). The T_c value increases for various end members of MPB solid solutions with $PbTiO_3$, decreasing the tolerance factor ($t_f \leq 1$). Therefore, the choice of low-tolerance-factor components such as $CaZrO_3$ could shift the T_c value to a higher temperature [11–14].

In this study, Ca^{2+} and Zr^{4+} are chosen as the dopants for $BaTiO_3$. Previous studies have investigated the position and function of Ca^{2+} and Zr^{4+} in $BaTiO_3$ [15–17]. Zr^{4+} (0.72 Å) tends to substitute the Ti-site (0.64 Å) of $BaTiO_3$ due to its ionic radius, which decreases the T_c value and increases the

*Corresponding authors. Tel.: +886 6 2754170; fax: +886 6 2380421.
E-mail addresses: a9007046@gmail.com (C.-Y. Chang), cyhuang@mail.ncku.edu.tw (C.-Y. Huang).

0272-8842/$ - see front matter
http://dx.doi.org/10.1016/j.ceramint.2013.04.009

orthorhombic phase transition temperature to a tetragonal one (T_{o-t}). Increasing T_{o-t} raises the dielectric constant of $BaTiO_3$ at room temperature. The ionic radius of Ca^{2+} (1.06 Å) is intermediate to those of the Ba-site (1.43 Å) and Ti-site (0.64 Å). In $BaTiO_3$, Ca^{2+} tends to substitute the Ba-site, which is also attributed to its ionic radius. The T_c value increases slightly when Ca^{2+} is substituted for the Ba-site. The T_c value decreases dramatically when Ca^{2+} is substituted for the Ti-site. Moreover, adding extra Ba^{2+} to $BaTiO_3$ moves Ca^{2+} from the Ba-site to the Ti-site and decreases the dielectric constant at the T_c value. Incorporating Ba^{2+} in the Ba-site shifts the primary Ca^{2+} to the Ti-site, which significantly alters both the unit cell volume and the T_c value. Hennings et al. found that excess Ba^{2+} moves Ca^{2+} from the Ba-site to the Ti-site [18]. Two extra Ba^{2+} are incorporated in the Ba-site for every Ca^{2+} in the Ti-site. Therefore, for each Ca^{2+} in the Ti-site, an oxygen vacancy is formed. In $BaTiO_3$, the Ca-acceptors are compensated by doubly ionized oxygen vacancies. The composition of BCTZ containing Ca^{2+} on the Ba-site and the Ti-site and oxygen vacancy is as follows:

$$(Ba_{1-x}Ca)(Ti_{1-y-p}Zr_yCa_P^{''})O_{3-p}V_{\ddot{O}}$$

The experiment in this study is divided into two parts. In the first part, Ca^{2+} and Zr^{4+} are chosen as the dopants in $BaTiO_3$ to produce a $(Ba_{0.95}Ca_{0.05})(Ti_{0.97}Zr_{0.03})O_3$ solid solution as the host. In the second part, Ca^{2+} is moved from the Ba-site to the Ti-site by adding Ba^{2+} to produce a $(Ba_{0.95+z}Ca_{0.05-d})(Ti_{0.97}Zr_{0.03}Ca_d)O_{3+z}$ solid solution. Dense ceramics with fine grains were obtained using a two-step sintering method. This study mainly focuses on investigating the effects of extra Ba^{2+} and two-step sintering on the crystal structure, microstructure, and dielectric properties of BCTZ.

2. Experimental procedure

The experimental procedure was divided into two parts: the preparation of the BCTZ powder and the preparation of the BCTZ powder with the addition of extra $BaCO_3$. In the first part, BCTZ ceramics were prepared via a solid-state reaction using high-purity commercial ($>99.9\%$) $BaCO_3$, TiO_2, $CaCO_3$, and ZrO_2 powders. The raw materials were dried, weighed, and ball-milled with distilled water and, subsequently, dried and calcined at various temperatures.

In the second part, single-phase BCTZ powder was chosen as the starting material. Two BCTZ powders with extra 4 and 6 mol% $BaCO_3$ were also prepared via a solid-state reaction method and were designated as BCTZ+4 and BCTZ+6, respectively. The calcined powders were milled and pressed into disks with a diameter of 8 mm and a thickness of 3 mm. The sintering shrinkage rates of the samples were determined by a dilatometer (DIL; Netzsch, 402C). The samples were heated to 1450 °C at a heating rate of 10 °C/min without dwelling. Based on the DIL results, the disks were sintered under normal and two-step sintering conditions. Fig. 1 shows the sintering profile for two-step sintering. The temperatures for the first step ($T1$) ranged from 1250 °C to 1300 °C, while the temperatures for the second step ($T2$) ranged from 1150 °C to 1200 °C. The heating rate from room temperature to $T1$ was 10 °C/min. The cooling rate from $T1$ to $T2$ was 30 °C/min. The dwelling time for the second step ($t2$) ranged from 8 h to 15 h. After sintering, the apparent densities of the samples were measured using the Archimedes method. Phase identification was then performed using an X-ray diffractometer (XRD; Siemens, D5000) and a Raman spectrometer (Microscopes Raman Spectrometer, Renishaw). Next, the cell parameters of all samples were determined based on the XRD results using cell parameter software [19]. The microstructures were observed via high-resolution scanning electronic microscopy (HR-SEM, Hitachi, SU8000). Additionally, the average grain size was evaluated from the SEM micrographs using Lucia measurement software (Laboratory Imaging, version 4.71). Each sample examined in this study contained at least 200 grains. For the dielectric measurements, an Ag-Pb paste was deposited on a plane parallel to the polished clean surfaces of ceramics, followed by heat treatment in air at 800 °C for 2 h. Furthermore, the temperature dependence of the capacitance of the samples from −55 °C to 150 °C was measured with an impedance analyzer LCR meter (HP 4284A) at 1 kHz.

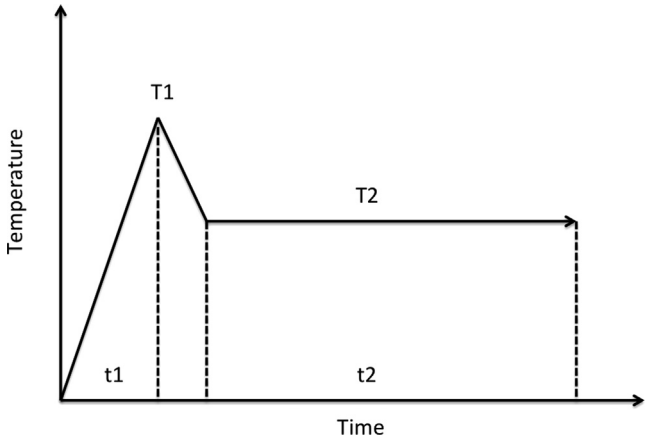

Fig. 1. Temperature program schedule for two-step sintering.

3. Results and discussion

Figs. 2 and 3 show the XRD patterns of BCTZ, BCTZ+4, and BCTZ+6 ceramics prepared via normal sintering and two-step sintering, respectively. The experimental results indicate that no secondary phases were found in any of the samples after sintering. Additionally, all samples exhibited a tetragonal phase, as evidenced by the splitting of the (103) and (301) diffraction peaks into a broad peak. The degree of splitting in the (103) and (301) diffraction peaks of the BCTZ ceramics prepared by normal sintering was slightly different from those prepared via two-step sintering. The difference in the degree of splitting between the two sintering methods was attributed to the increase in crystallinity. The samples prepared by normal sintering exhibited higher grain sizes, which also increased their crystallinity. Therefore, the BCTZ ceramics prepared by normal sintering might have a higher crystallinity than that prepared by two-step sintering.

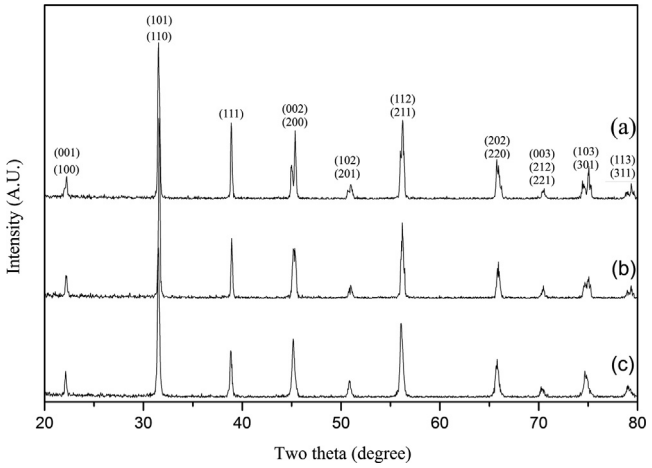

Fig. 2. XRD patterns of (a) BCTZ, (b) BCTZ+4, and (c) BCTZ+6 sintered at 1300 °C/4 h.

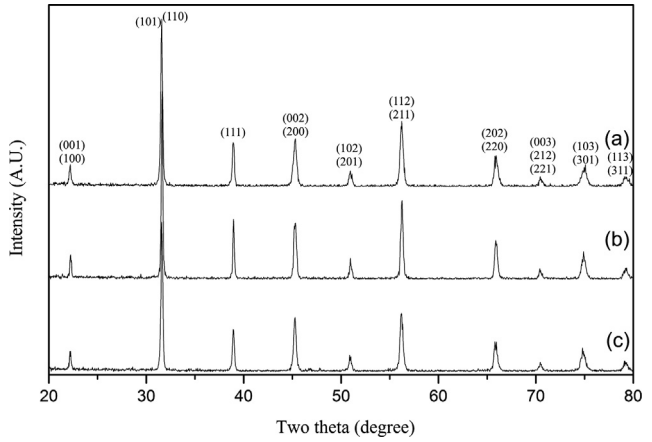

Fig. 3. XRD patterns of (a) BCTZ, (b) BCTZ+4 sintered at 1250 °C/1 min–1200 °C/8 h, and (c) BCTZ+6 sintered at 1300 °C/1 min–1200 °C/8 h.

With the incorporation of additional Ba^{2+}, the XRD patterns of BCTZ+4 and BCTZ+6 both shifted to a low 2θ values compared with BCTZ. Shifts in the XRD patterns were also observed in the samples prepared by normal sintering and two-step sintering. This shift in the XRD patterns was attributed to the substitution of Ca^{2+} from the Ba-site to the Ti-site. As mentioned earlier, the ionic radius of Ca^{2+} (1.06 Å) is between those of the Ba-site (1.43 Å) and Ti-site (0.64 Å). When Ca^{2+} was forced into the Ti-site, the unit cell expanded and the *d*-spacing increased. Therefore, the XRD patterns of BCTZ+4 and BCTZ+6 shifted to a low 2θ value. Table 1 lists the cell parameters and tetragonality of the samples prepared by normal sintering and two-step sintering. The experimental results indicate that when incorporating additional Ba^{2+}, the *a*-axis increased, the *c*-axis decreased, and the tetragonality decreased. The decrease in tetragonality may be due to the substitution of Ca^{2+} in both the Ba-site and the Ti-site as well as the substitution of Zr^{4+} in the Ti-site in $BaTiO_3$.

Figs. 4 and 5 show the Raman spectra of BCTZ, BCTZ+4, and BCTZ+6 prepared by normal sintering and two-step sintering. Optical phonon modes at 306 cm^{-1} [B1, E (TO_3+LO_2)], 516 cm^{-1} [E (TO), A_1 (TO)], and 712 cm^{-1} [E (LO_4), A_1 (LO_3)] were found in single tetragonal $BaTiO_3$ crystals. According to Figs. 4 and 5, all Raman peaks were assigned to those of the tetragonal P4*mm* symmetry [20]. Almost the same Raman bands were observed in the BCTZ, BCTZ+4, and BCTZ+6 ceramics after sintering, explaining why the crystalline phases of all BCTZ samples were tetragonal. The Raman spectra reveal that the peak intensities at 300 cm^{-1} and 717 cm^{-1} both decreased when additional Ba^{2+} was incorporated, which may be caused by the

Table 1
Cell parameters and tetragonality of BCTZ, BCTZ+4, and BCTZ+6 with normal sintering and two-step sintering methods. The number in the parenthesis respresent the erro of the cell parameters.

	BCTZ	BCTZ+4	BCTZ+6
Cell parameters and tetragonality after normal sintering			
a-axis (Å)	4.0125(8)	4.0219(7)	4.0081(8)
c-axis (Å)	4.0419(9)	4.0416(9)	4.0232(9)
Tetragonality	1.0073	1.0049	1.0038
Cell parameters and tetragonality after two-step sintering			
a-axis (Å)	3.9982(4)	4.0050(9)	4.0121(9)
c-axis (Å)	4.0301(5)	4.0211(8)	4.0193(8)
Tetragonality	1.0079	1.0040	1.0018

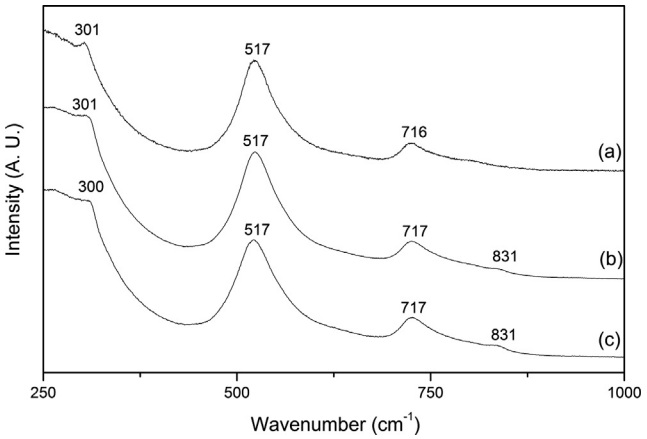

Fig. 4. Raman spectra of (a) BCTZ, (b) BCTZ+4, and (c) BCTZ+6 sintered at 1300 °C/4 h.

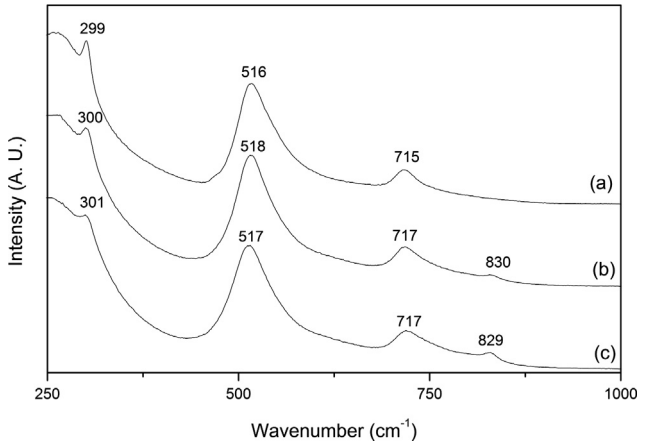

Fig. 5. Raman spectra of (a) BCTZ, (b) BCTZ+4 sintered at 1250 °C/1 min–1200 °C/8 h, and (c) BCTZ+6 sintered at 1300 °C/1 min–1200 °C/8 h.

reduced tetragonality when Ca^{2+} was substituted in the Ti-site. Moreover, the Raman peak at 830 cm^{-1} was observed in BCTZ +4 and BCTZ+6 prepared via two different sintering methods. This higher-frequency Raman peak was also observed in Ba$(Ti_{0.985}Ca_{0.005}Nb_{0.01})O_3$ ceramics, which were fabricated by co-incorporating cations (Ca and Nb) at the Ti-sites of $BaTiO_3$ [21]. Based on previous studies, this Raman peak indicates the formation of Ca_{Ti} defects, which are attributed to the transformation of Ca^{2+} from the Ba-site to the Ti-site when additional Ba^{2+} is incorporated. This phenomenon also explains the shift in the XRD patterns of BCTZ+4 and BCTZ+6, as shown in Figs. 2 and 3. Therefore, in addition to determining the crystalline phase, the Raman spectra confirm that Ca^{2+} can be forced into the Ti-site when additional Ba^{2+} is incorporated via the two different sintering methods.

Fig. 6 shows the sintering shrinkage curves for BCTZ, BCTZ+4, and BCTZ+6. Increasing the Ba^{2+} concentration shifted the shrinkage curves to a higher temperature, indicating that BCTZ with extra Ba^{2+} required a higher densification temperature or a longer dwelling time than BCTZ. Table 2 summarizes the average grain sizes and relative densities for different normal sintering temperatures. For all of the samples, the average grain size and relative density both increased with increasing sintering temperature. This table also revealed grain growth inhibition in the BCTZ+4 and BCTZ+6 samples. This phenomenon suggests that the first few percentages of Ca^{2+} added could be dissolved into the $BaTiO_3$ matrix to replace Ba^{2+} and Ti^{4+}. Moreover, Ca^{2+} may be found at the grain boundary region and may suppress grain growth only when the amount of Ca^{2+} added exceeds the solubility of the $BaTiO_3$.

Table 3 lists the average grain sizes and relative densities under various two-step sintering conditions. The dwelling time

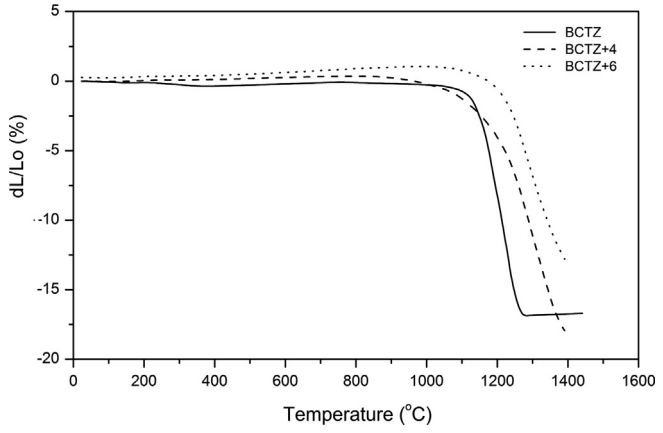

Fig. 6. Sintering shrinkage curves of BCTZ, BCTZ+4, and BCTZ+6.

Table 2
Average grain size and relative density with various normal sintering temperatures.

	BCTZ	BCTZ+4	BCTZ+6
1250 °C/4 h	5.52 μm (92.1%)	4.23 μm (91.7%)	2.25 μm (93.0%)
1300 °C/4 h	7.21 μm (95.3)%	5.31 μm (93.1%)	5.42 μm (94.3%)
1350 °C/4 h	10.42 μm (97.2%)	9.71 μm (94.2%)	6.71 μm (96.6%)

(8 h to 15 h) at $T2$ did not significantly affect the relative densities of all samples; however, the relative densities increased with increasing $T2$. Moreover, the average grain size was still less than 0.5 μm under various two-step sintering conditions. Fig. 7(a) to (f) show the SEM micrographs of BCTZ, BCTZ+4, and BCTZ+6 sintered under different sintering methods. The average grain size of the sample under normal sintering (i.e., approximately 3 μm to 10 μm) was greater than that prepared by two-step sintering (i.e., less than 0.5 μm). Two-step sintering successfully inhibited grain growth during the final stage of the sintering process. A fine-grain microstructure can thus be obtained using two-step sintering with average grain sizes below 0.5 μm in all samples.

Fig. 8(a) and (b) show the temperature dependence of the capacitance (TCC) and dielectric constants of BCTZ, BCTZ +4, and BCTZ+6 ceramics prepared by normal sintering. The TCC peaks correspond to the phase transition temperature of each sample, as shown in Fig. 8(a). Two phase transition temperatures can be found in the BCTZ ceramics: T_c (approximately 125 °C) and the phase transition from orthorhombic to tetragonal (i.e., T_{o-t}, which is approximately 30 °C). In contrast to pure $BaTiO_3$, the T_c value of BCTZ prepared by normal sintering did not change significantly. However, the T_{o-t} value of BCTZ prepared by normal sintering increased from 0 °C to 30 °C. The increase in T_{o-t} was attributed to the substitution of Zr^{4+} in the Ti-site [15]. As extra Ba^{2+} was added, the T_c value of BCTZ+4 decreased slightly from 125 °C to 110 °C, as shown in Fig. 8(a) and (b). The decrease in T_c was due to the substitution of Ca^{2+} in the Ti-site when extra Ba^{2+} was added. Additionally, increasing the amount of extra Ba^{2+} to 6 mol% moved more Ca^{2+} from the Ba-site to the Ti-site. Moreover, the Ca^{2+} concentration in the Ti-site increased, which decreased the T_c value of BCTZ+6 from 110 °C to 75 °C. A broad peak was observed in the BCTZ+6 sample, as shown in Fig. 8(a) and (b). The broad TCC peak was caused by the combination of T_c and T_{o-t} when Ca^{2+} was substituted in both the Ba-site and the Ti-site. The high dielectric constant of BCTZ+6 prepared by normal sintering was also due to the combination of T_c and T_{o-t} when Ca^{2+} was substituted in both the Ba-site and the Ti-site. Fig. 8(c) shows the temperature dependence of the tanδ of BCTZ, BCTZ+4, and BCTZ+6 prepared by normal sintering. The experimental results indicate that the dielectric loss increased as extra Ba^{2+} was added. The curve of the temperature dependence of tanδ warped upwards when the temperature exceeded 100 °C, which, based on a previous study, was attributed to the migration of oxygen vacancies when Ca^{2+} is substituted in the Ti-site [22].

Fig. 9(a) and (b) show the temperature dependence of the capacitances and the dielectric constants of BCTZ, BCTZ+4, and BCTZ+6 ceramics prepared by two-step sintering. Two phase transition temperatures can be observed for the BCTZ and BCTZ+4 ceramics: T_c (approximately 125 °C) and T_{o-t} (approximately 35 °C). Shifts in the T_{o-t} value of the BCTZ and BCTZ+4 ceramics were also attributed to the substitution of Zr^{4+} in the Ti-site. As extra Ba^{2+} was added, the T_c value of BCTZ+4 decreased slightly from 125 °C to 115 °C, as shown

Table 3
Average grain size and relative density with various two-step sintering conditions. ($T1 = 1250$ °C and $T2 = 1150$–1200 °C).

	BCTZ	BCTZ+4	BCTZ+6
1250 °C/1 min–1150 °C/8 h	0.21 μm (90.2%)	0.31 μm (94.2%)	0.24 μm (85.9%)
1250 °C/1 min–1150 °C/15 h	0.24 μm (91.0%)	0.32 μm (94.7%)	0.25 μm (87.5%)
1250 °C/1 min–1200 °C/8 h	0.25 μm (96.2%)	0.49 μm (98.5%)	0.30 μm (91.4%)

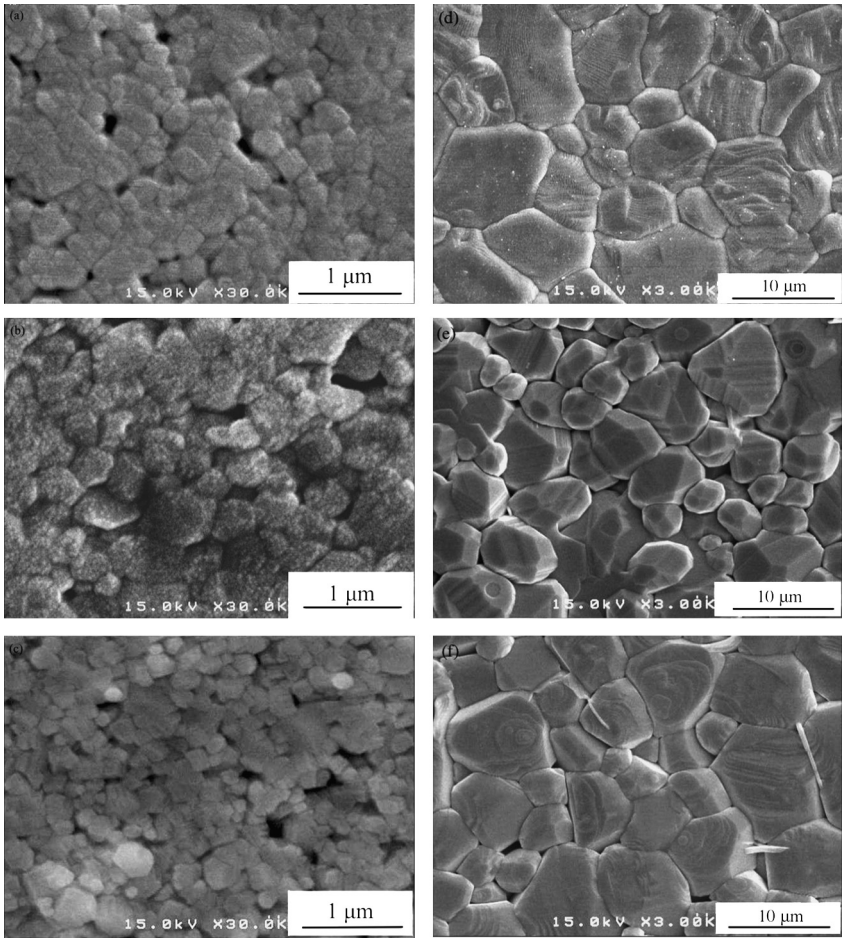

Fig. 7. SEM micrographs of BCTZ, BCTZ+4, and BCTZ+6 sinter bulks (a) BCTZ, (b) BCTZ+4 sintered at 1250 °C/1 min–1200 °C/8 h, (c) BCTZ+6 sintered at 1300 °C/1 min–1200 °C/8 h, (d) BCTZ, (e) BCTZ+4, and (f) BCTZ+6 sintered at 1300 °C/4 h.

in Fig. 9(a) and (b). The decrease in T_c was also attributed to the substitution of Ca^{2+} in the Ti-site when extra Ba^{2+} was added. The TCC curve of the BCTZ+6 ceramics shows a flattened peak, and the phase transition temperature was difficult to determine. As mentioned earlier, when extra Ba^{2+} was added, more Ca^{2+} was pushed from the Ba-site to the Ti-site, subsequently decreasing T_c. The broad TCC curve of the BCTZ+6 ceramic was caused by the combination of T_c and T_{o-t} when Ca^{2+} was substituted in both the Ba-site and the Ti-site and when Zr^{4+} was substituted in the Ti-site. Moreover, the flattening of the TCC curve of the BCTZ+6 ceramic may be attributed to increased internal stress with decreasing grain sizes (approximately 0.3 μm). Therefore, the stable temperature dependence of the capacitance with the dielectric peak was inhibited at T_c over a wide temperature range due to the increase in internal stress. Comparing the temperature dependences of the dielectric constants revealed that the BCTZ+6 ceramic prepared via two-step sintering had a low dielectric constant. As mentioned earlier, the fine-grain microstructure can be obtained using two-step sintering. Moreover, the substitution of Ca^{2+} in the Ti-site decreases its tetragonality. The decrease in grain size and tetragonality further decreased the spontaneous polarization and permittivity. Therefore, BCTZ+6 prepared by two-step sintering exhibited a lower permittivity than that prepared by normal sintering. Fig. 9(c) shows the temperature dependence of the tanδ of BCTZ, BCTZ+4, and BCTZ+6 prepared by two-step sintering. The tanδ of BCTZ+6 prepared via two-step sintering was lower than that prepared via normal sintering (Fig. 8(c)), possibly owing to the difference in grain sizes because the samples were prepared by different sintering methods. Based on the average grain size in Tables 2 and 3, the BCTZ+6

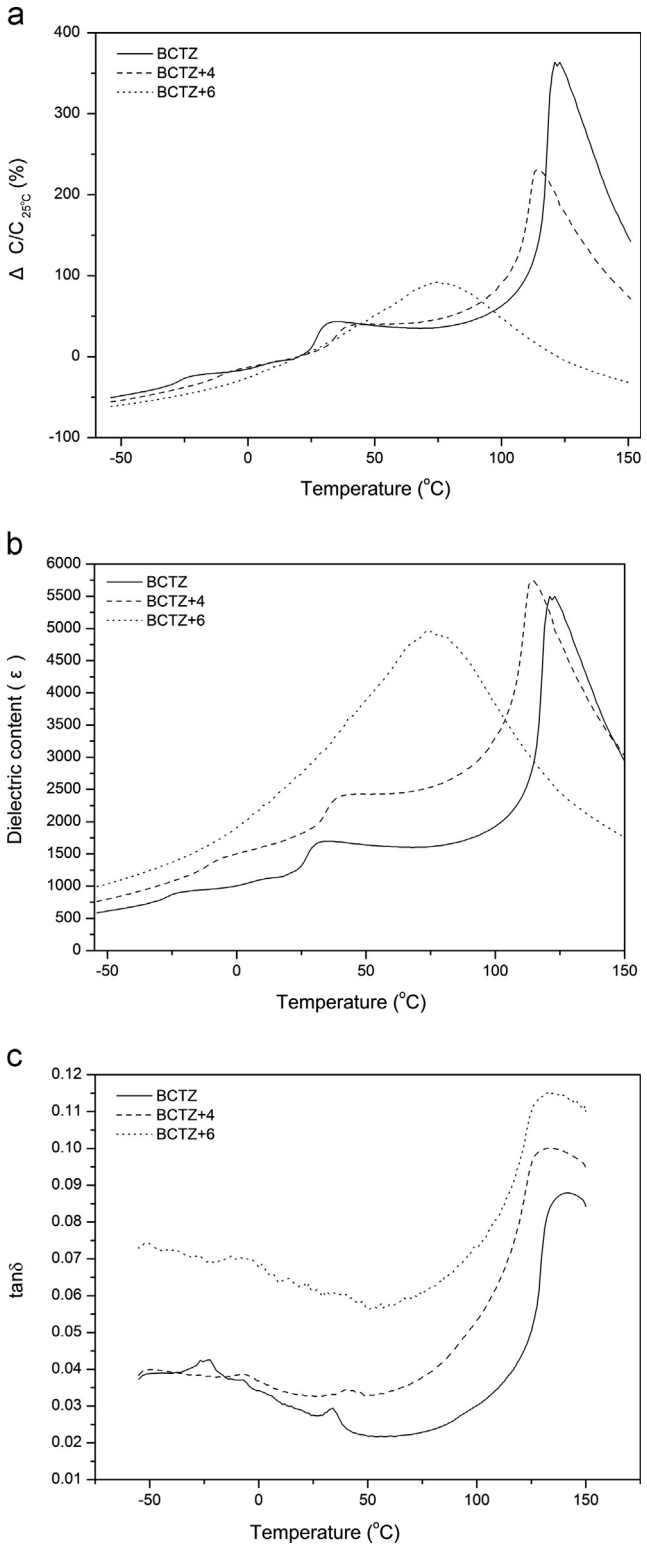

Fig. 8. (a) Temperature dependence of capacitance curves, (b) temperature dependence of dielectric constant curves, and (c) the tanδ at 25 °C of BCTZ, BCTZ+4 and BCTZ+6 sintered at 1300 °C/4 h.

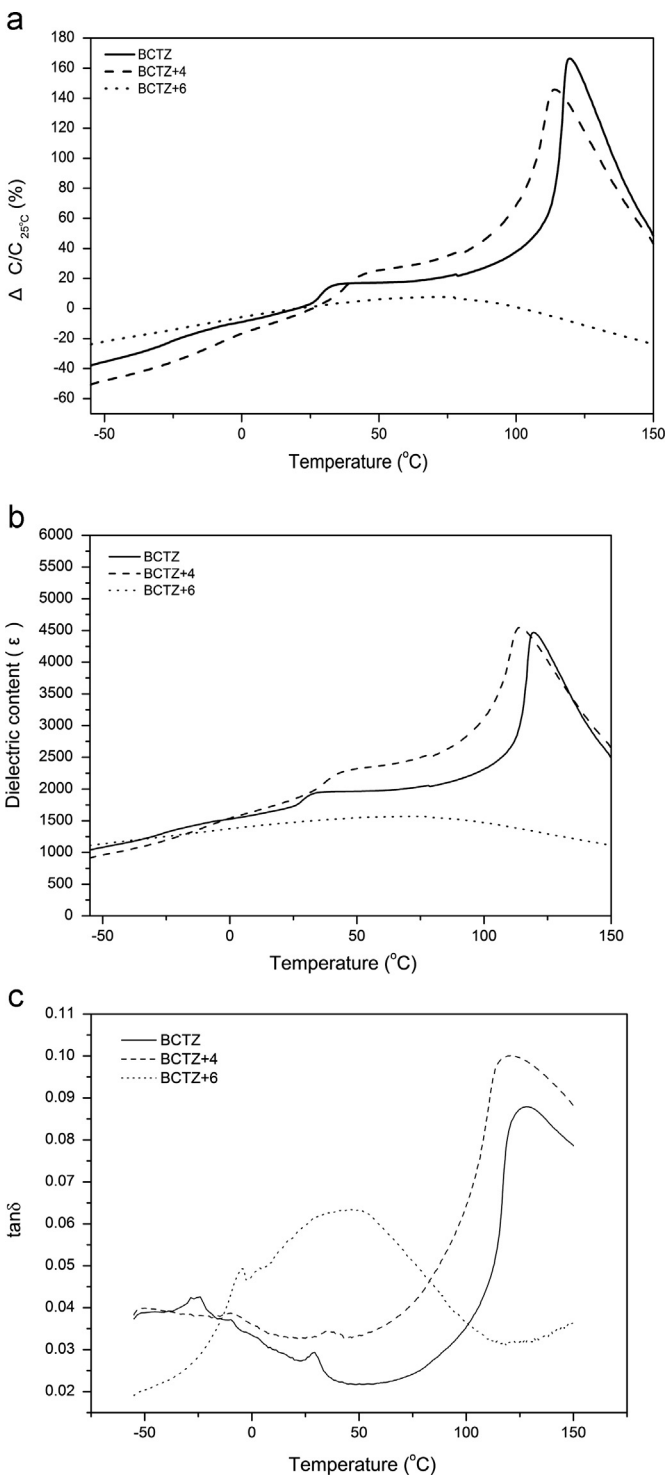

Fig. 9. (a) Temperature dependence of the capacitance curves, (b) temperature dependence of the dielectric constant curves, and (c) tanδ at 25 °C of BCTZ and BCTZ+4 sintered at 1250 °C/1 min–1200 °C/8 h and BCTZ+6 sintered at 1300 °C/1 min–1200 °C/8 h.

prepared via normal sintering had a larger grain size than that prepared by two-step sintering. Therefore, the tanδ of BCTZ +6 prepared via normal sintering was higher than that prepared by two-step sintering.

4. Conclusions

The XRD results demonstrate that all BCTZ samples comprise a single phase. The Raman spectra defined the crystalline phase and confirmed that Ca^{2+} can be forced into

the Ti-site by adding extra Ba^{2+}. The TCC curves reveal that the T_c value of all BCTZ samples shifted to lower temperatures when extra Ba^{2+} was added. The SEM micrographs indicate that all of the BCTZ samples prepared by two-step sintering (1250 °C/1 min–1200 °C/8 h and 1300 °C/1 min–1200 °C/8 h) had a fine grain microstructure (grain size < 0.5 μm) and a high density (i.e., relative density $> 95\%$) Moreover, the capacitance curves of the BCTZ samples with a fine grain microstructure had a flattened temperature coefficient. Importantly, in addition to determining the effects of additional Ba^{2+} on BCTZ, this study demonstrated that flattened TCC curves can be achieved when two-step sintering was performed.

Acknowledgements

The authors would like to thank the National Science Council of the Republic of China, Taiwan, for financially supporting this research under Contract No. NSC NSC100-2221-E-006-134-MY3.

References

[1] G. Arlt, D. Hennings, G.D. With, Dielectric properties of fine-grained barium titanate ceramics, Journal of Applied Physics 58 (1985) 1619–1625.
[2] I.W. Chen, X.H. Wang, Sintering dense nanocrystalline ceramics without final-stage grain growth, Nature 9 (2000) 404.
[3] X.H. Wang, X.Y. Deng, H.L. Bai, H. Zhou, W.G. Qu, L.T. Li, Two-step sintering of ceramics with constant grain-size II: $BaTiO_3$ and Ni–Cu–Zn ferrite, Journal of the American Ceramic Society 89 (2006) 438–443.
[4] Y.H. Han, J.B. Appleby, D.M. Smyth, Calcium as an acceptor impurity in $BaTiO_3$, Journal of the American Ceramic Society 70 (1987) 96–100.
[5] J.G. Park, T.S. Oh, Y.H. Kim, Dielectric properties and microstructural behavior of B-site calcium-doped barium titanate ceramics, Journal of Materials Science 27 (1992) 5713–5719.
[6] B. Tang, S.R. Zhang, Y. Yuan, X.H. Zhou, Y.S. Liang, Influence of $CaZrO_3$ on dielectric properties and microstructures of $BaTiO_3$-based X8R ceramics, Science in China Series E: Technological Sciences 51 (2008) 1451–1456.
[7] D. Hennings, A. Schnell, Diffuse ferroelectric phase transitions in $Ba(Ti_{1-y}Zr_y)O_3$, Journal of the American Ceramic Society 65 (1982) 539–544.
[8] R.E. Eitel, C.A. Randall, T.R. Shrout, P.W. Rehrig, W. Hankenberger, S.E. Park, New High temperature morphotropic phase boundary piezoelectrics based on $Bi(Me)O_3$—$PbTiO_3$ ceramics, Japanese Journal of Applied Physics 40 (2001) 5999–6002.
[9] L. Chen, L. Li, X. Wang, Z. Tian, Z. Gui, The study of Ca- doped BCTZ ceramics sintered in reducing atmosphere, Journal of Electroceramics 22 (2008) 569–572.
[10] L. Zhang, O.P. Thakur, A. Feteira, G.M. Keith, A.G. Mould, D.C. Sinclair, A.R. West, Comment on the use of calcium as a dopant in X8R BaTiO3-based ceramics, Applied Physics Letters 90 (2007) 142914-1-142914-3.
[11] S. Lee, R.W.H. Woodford, C.A. Randall, Crystal and defect chemistry influences on band gap trends in alkaline earth perovskites, Applied Physics Letters 92 (2008) 201909-1-201909-3.
[12] S. Lee, C.A. Randall, A modified Vegard's law for multisite occupancy of Ca in $BaTiO_3$–$CaTiO_3$ solid solutions, Applied Physics Letters 92 (2008) 111904-1-11904-3.
[13] P. Hansen, D. Hennings, H. Schreineacher, High-K dielectric ceramics from donor/acceptor-codoped $(Ba_{1-x}Ca_x)(Ti_{1-y}Zr_y)O_3$, Journal of the American Ceramic Society 81 (1998) 1369–1373.
[14] N. Sakurai, V. Bojan, J.J. Stapleton, G.Y. Yang, C.A. Randall, Y. Mizuno, H. Chazono, Surface instability in high surface area complex oxides-$BaTiO_3$ study, Japanese Journal of Applied Physics 48 (2009) 061404-1-061404-7.
[15] S.J. Kuang, X.G. Tang, L.Y. Li, Y.P. Jiang, Q.X. Liu, Influence of Zr dopant on the dielectric properties and Curie temperatures of $Ba(Zr_xTi_{1-x})O_3$ ($0 \le x \le 0.12$) ceramics, Scripta Materialia 61 (2009) 68–71.
[16] M.S. Yoon, S.C. Ur, Effects of A-site Ca and B-site Zr substitution on dielectric properties and microstructure in tin-doped $BaTiO_3$–$CaTiO_3$ composites, Ceramics International 34 (2008) 1941–1948.
[17] B. Jaffe Jr., W.R. Cook, H. Jaffe, Piezoelectric Ceramics, first ed., Academic Press, London, 1971.
[18] D.F.K. Hennings, H. Schreinemacher, Ca-acceptors in dielectric ceramics sintered in reducive atmospheres, Journal of the European Ceramic Society 15 (1995) 795–800.
[19] C.Y. Huang, Thermal Expansion Behavior of Sodium Zirconium Phosphate Structure Type materials, Ph.D. Thesis, The Pennsylvania State University, U.S.A., 1990.
[20] P.S. Dobal, A. Dixit, R.S. Katiyar, Micro-Raman scattering and dielectric investigations of phase transition behavior in the $BaTiO_3$–$BaZrO_3$ system, Journal of Applied Physics 89 (2001) 8085–8091.
[21] M.C. Chang, S.C. Yu, Raman study for $(Ba_{1-x}Ca_x)TiO_3$ and $Ba(Ti_{1-y}Ca_y)O_3$ crystalline ceramics, Journal of Materials Science Letters 19 (2000) 1323–1325.
[22] Z. Yu, C. Ang, R. Guo, A.S. Bhalla, Dielectric properties of $Ba(Ti_{1-x}Zr_x)O_3$ solid solutions, Materials Letters 61 (2007) 326–329.